Oscillator strengths and line widths of dipole-allowed transitions in $^{14}N_2$ between 89.7 and 93.5 nm

G. Stark,[1,a)] B. R. Lewis,[2] A. N. Heays,[2] K. Yoshino,[3] P. L. Smith,[3] and K. Ito[4]
[1]*Department of Physics, Wellesley College, Wellesley, Massachusetts 02481, USA*
[2]*Research School of Physical Sciences and Engineering, The Australian National University, Canberra, ACT 0200, Australia*
[3]*Harvard-Smithsonian Center for Astrophysics, Cambridge, Massachusetts 02138, USA*
[4]*Photon Factory, Institute for Materials Structure Science, High Energy Accelerator Research Organization, 1-1 Oho, Tsukuba, Ibaraki 305-0801, Japan*

(Received 20 November 2007; accepted 21 December 2007; published online 17 March 2008)

Line oscillator strengths in the 20 electric dipole-allowed bands of $^{14}N_2$ in the 89.7–93.5 nm (111480–106950 cm^{-1}) region are reported from photoabsorption measurements at an instrumental resolution of ~6 mÅ (0.7 cm^{-1}) full width at half maximum. The absorption spectrum comprises transitions to vibrational levels of the $3p\sigma_u$ c_4' $^1\Sigma_u^+$, $3p\pi_u$ c_3 $^1\Pi_u$, and $3s\sigma_g$ o_3 $^1\Pi_u$ Rydberg states and of the b' $^1\Sigma_u^+$ and b $^1\Pi_u$ valence states. The J dependences of band f values derived from the experimental line f values are reported as polynomials in $J'(J'+1)$ and are extrapolated to $J'=0$ in order to facilitate comparisons with results of coupled Schrödinger-equation calculations. Most bands in this study are characterized by a strong J dependence of the band f values and display anomalous P-, Q-, and R-branch intensity patterns. Predissociation line widths, which are reported for 11 bands, also exhibit strong J dependences. The f value and line width patterns can inform current efforts to develop comprehensive spectroscopic models that incorporate rotational effects and predissociation mechanisms, and they are critical for the construction of realistic atmospheric radiative-transfer models. © *2008 American Institute of Physics*. [DOI: 10.1063/1.2834933]

I. INTRODUCTION

Photoexcitation and electron impact excitation of molecular nitrogen in the extreme ultraviolet spectral region (EUV) ($\lambda < 100$ nm) initiate critical dissociation and ionization processes in the Earth's upper atmosphere and in other nitrogen-rich planetary atmospheres. EUV and vacuum ultraviolet N_2 airglow emissions are observed in the terrestrial atmosphere,[1–3] as well as in the atmospheres of Titan[4–6] and Triton.[7] The interpretation of atmospheric and interstellar[8] observations and the modeling of upper atmospheric processes[9,10] require a detailed understanding of the EUV photoabsorption spectrum of $^{14}N_2$ and its isotopic variants. EUV transmission models through N_2-rich atmospheres[11] and airglow radiative-transfer models require a comprehensive and complete database of line positions, line oscillator strengths, and line widths. We report here line oscillator strengths in 20 bands of $^{14}N_2$ in the 89.7–93.5 nm (111480–106950 cm^{-1}) region and predissociation line widths in 11 bands. This work is a continuation of our measurement program to survey, at high resolution, the electric-dipole-allowed photoabsorption spectrum of N_2 from its onset at 99.5 nm to the first ionization limit at 79.6 nm; it extends to shorter wavelengths, and the results are presented in the study of Stark *et al.*[12] for the 93.5–99.5 nm region. The bands studied include transitions between the ground state $X(0)$ and the vibronic upper states $b(9-14)$, $b'(5-11)$, $c_4'(2,3)$, $c_3(2,3)$, and $o_3(1-3)$.

The electric-dipole-allowed absorption spectrum of N_2 shortward of 100 nm arises from transitions to the strongly perturbed vibrational progressions of three Rydberg and two valence states.[13–15] c_4' $^1\Sigma_u^+$ and c_3 $^1\Pi_u$ are the lowest members ($n=3$) of the $np\sigma_u$ and $np\pi_u$ Rydberg series converging to the X $^2\Sigma_g^+$ ground state of N_2^+; the o_3 $^1\Pi_u$ state is the $n=3$ lowest member of the $ns\sigma_g$ series converging to A $^2\Pi_u$ of N_2^+; and b $^1\Pi_u$ and b' $^1\Sigma_u^+$ are valence states. Stahel *et al.*[16] reproduced the anomalous absorption strength patterns observed within the vibrational progressions by treating the homogeneous Rydberg-Rydberg and Rydberg-valence interactions among the five electronic states. Observed vibronic term values and rotational constants[17–19] and relative dipole strengths determined from electron energy-loss spectra[20] were used to optimize a set of electronic transition moments derived from electronically coupled diabatic potential curves. Spelsberg and Meyer[21] refined the analysis of Stahel *et al.*[16] by combining *ab initio* potential curves with electronic couplings dependent on the internuclear distance R.

Lewis *et al.*[22] developed a quantitative model for the b, c_3, and o_3 $^1\Pi_u$ states that clarifies the predissociation mechanisms affecting the photoabsorption spectrum. Their coupled-channel Schrödinger equation (CSE) model of the b, c_3, and o_3 interactions with the C and C' $^3\Pi_u$ states, optimized using the experimental database of isotope-dependent line positions and line widths, reproduces the low-rotation line broadenings observed in the $^{14}N_2$, $^{15}N_2$, and $^{14}N^{15}N$ $^1\Pi_u$ vibrational levels below 105 350 cm^{-1}. Their model calculation shows that the spin-orbit interaction between the b $^1\Pi_u$

a)Electronic mail: gstark@wellesley.edu.

and $C\ ^3\Pi_u$ levels, along with an electrostatic interaction between the C state and the continuum of $C'\ ^3\Pi_u$, accounts for the observed line-broadening patterns. In an extension of the $^1\Pi_u$ and $^3\Pi_u$ CSE model of Lewis *et al.*,[22] the measured rotational effects in line strengths and predissociation line widths in the $X(0)\rightarrow{}^1\Pi_u$ vibrational bands, reported in our earlier work,[12] were modeled successfully by Haverd *et al.*[23] A further extension of the CSE model, which includes the $F\ ^3\Pi_u$ and $G\ ^3\Pi_u$ Rydberg states[24–26] and which incorporates heterogeneous interactions of the $^{1,3}\Pi_u$ manifold with the $c_4'\ ^1\Sigma_u^+$ and $b'\ ^1\Sigma_u^+$ states, is under development.[27] A version of the extended CSE model was used recently to calculate nitrogen isotopic fractionation in the atmosphere of Titan,[10] as well as to elucidate the radiative properties of the $c_4'\ ^1\Sigma_u^+\leftarrow X\ ^1\Sigma_g^+$ band system.[28]

Early optical measurements of N_2 band oscillator strengths at EUV wavelengths,[29–31] reviewed in Stark *et al.*,[12] were compromised by saturation effects associated with insufficient spectral resolution. Electron-scattering measurements, which are not subject to the saturation effects that complicate the interpretation of optical measurements, include those of Geiger and Schröder,[20] who reported relative intensities in the N_2 energy-loss spectrum of 25 keV electrons at a resolution of 10 meV ($\sim$80 cm^{-1}) full width at half maximum (FWHM); Chan *et al.*,[32] who determined absolute N_2 band f values from energy-loss spectra of 8 keV electrons at a resolution of 48 meV ($\sim$400 cm^{-1}) FWHM; and Ajello *et al.*[33] and James *et al.*,[34] who reported band f values derived from emission-excitation cross section measurements. Early measurements of predissociation line broadening in the N_2 EUV bands[15,35,36] have been supplanted by an extensive program of laser-based line width and lifetime measurements by Ubachs and co-workers.[37–48] The predissociation line width database developed from the measurements of Ubachs and co-workers, along with far more limited line width measurements of the broader N_2 features by Stark *et al.*,[12] has informed the development of the CSE predissociation models of Lewis and co-workers.[22,23]

The strong Rydberg-Rydberg, Rydberg-valence, and valence-valence interactions among the singlet and triplet states of N_2 produce striking rotation-dependent effects on line strengths and widths. In the spectral region studied in this report, Carroll and Collins[15] first identified a number of anomalous line strength patterns in the $b(v)-X(0)$ bands, Walter *et al.*[49] reported departures from normal rovibrational intensity patterns in photofragment signals following laser excitation of the $c_4'(3)$, $c_3(3)$, and $b'(10)$ levels, and rotation-dependent lifetimes were reported for the $c_4'(2)$ level.[41] Ajello *et al.*[50] derived J-dependent predissociation yields in the $c_4'(3)$ level from emission intensities following electron-impact excitation. Vieitez *et al.*[51] recently analyzed the unusual rotational patterns in the line strengths and predissociation line widths of the $o_3(1)-X(0)$ and $b(9)-X(0)$ bands seen in laser-based ionization spectroscopy and synchrotron-based photoabsorption spectra. Throughout the 89.7 to 93.5 nm region, heterogeneous interactions are responsible for many of the rotation-dependent effects. Edwards *et al.*,[52] Ubachs *et al.*,[41] and Walter *et al.*[49] extended the treatment of Stahel *et al.*[16] by including the effects of rotation to interpret the observed J dependences of emission intensities, lifetimes, and predissociation yields.

Rotation-dependent effects are widely spread throughout the near-threshold region of N_2. Of the 20 bands presented in this report, all but two show nonstandard line intensity and/or line width patterns. The J dependences of the line oscillator strengths and predissociation line widths have been extrapolated to $J'=0$, allowing for direct comparisons with CSE molecular models[16,21,22] that do not account for rotational effects. Polynomial fits to the J-dependent patterns, presented in Table I, can inform more comprehensive models (e.g., Haverd *et al.*[23]) that incorporate rotational effects. Our measurements also provide a further experimental foundation for the development of models that include higher-lying levels in the $^{1,3}\Pi_u$ manifold along with heterogeneous interactions with higher-lying $^1\Sigma_u^+$ and $^3\Sigma_u^+$ levels.

II. EXPERIMENTAL PROCEDURE

A detailed description of the experimental procedure is presented in Ref. 12. A brief summary follows.

Photoabsorption measurements were undertaken at the 2.5 GeV storage ring of the Photon Factory, a synchrotron radiation facility at the High Energy Accelerator Research Organization in Tsukuba, Japan. A 6.65 m spectrometer with a focal plane scanner[53,54] provided high spectral resolution. A zero-dispersion order sorter reduced the bandpass of the continuum radiation entering the spectrometer to about 3 nm. A 1200 grooves mm^{-1} grating, blazed at 550 nm, was used in the sixth order to give a reciprocal dispersion of $\sim$0.02 nm mm^{-1}; spectrometer entrance and exit slits of $\sim$10 μm resulted in an instrumental resolution of about 6×10^{-4} nm (0.7 cm^{-1}) FWHM. The spectrometer tank, at a temperature of 295 K, served as an absorption cell with a path length of $\sim$12.5 m; the exact value depends on the grating position and was calculated for each absorption band. Absorption spectra were recorded at tank pressures ranging from 8.4×10^{-6} to 1.2×10^{-4} torr, corresponding to N_2 column densities ranging from 2.7×10^{14} to 4.4×10^{15} cm^{-2}. The spectrometer tank pressure was monitored with an ionization gauge. The gauge was calibrated by volumetric expansion of N_2; a small volume, representing a measured fraction of the spectrometer tank volume and filled to pressures that could be measured with a capacitance manometer, was expanded into the main tank. N_2 was used in natural isotopic abundance ($^{14}N_2$ 99.3%, $^{14}N^{15}N$ 0.7%).

The bands were scanned at speeds ranging from 0.0025 to 0.006 nm min^{-1}; signal integration times of $\sim$1 s then resulted in one data point for each 4.4×10^{-5} to 1.06×10^{-4} nm interval of the spectrum. Most bands were scanned in two or three overlapping portions, typically of 0.1 nm width. Signal rates from the detector, a windowless solar-blind photomultiplier tube with a CsI-coated photocathode, were $\sim$50 000 s^{-1} for the background continuum; the detector dark count rate was less than 2 s^{-1}. Typically, a signal-to-noise ratio of $\sim$250 was achieved for the background continuum level.

TABLE I. Summary of measured f values and line widths for EUV transitions from $X(0)$ of $^{14}N_2$. Uncertainties (in parentheses; 1 standard error) are in units of the last-quoted decimal place. The measured oscillator strengths are reported in terms of a "rotationless" band f value $f(J'=0)$ and a polynomial in $x=J'(J'+1)$ that represents the rotational dependence of band f values $f(J')$ derived from line f values. The parameters $\Gamma(J'=0)$ and $\Gamma(J')$ are used to report the Lorentzian components (FWHM) of the measured line widths. Γ_{lit} refers to data taken from the literature (Refs. 38, 41, 43–45, 48, and 65).

Band	$T(\nu_0)$ (cm^{-1})	No. of lines	Observed J' range	$f(J'=0)$ ($\times 10^3$)	$f(J')$ ($\times 10^3$)	$\Gamma(J'=0)$ (cm^{-1})	$\Gamma(J')$ (cm^{-1})	Γ_{lit} (cm^{-1})
$b'(5)-X(0)$	107 326	34	0–19	1.1(1)	P: $1.12+0.0014x$ R: $1.12-0.0012x$			0.025(3)
$o_3(1)$[a]	107 636	58	1–26	3.0(3)		0.27(5)	$0.27-(3\times10^{-4})x$	
$b(9)$[a]	107 648	43	1–20	14(2)		0.21(5)		
$b'(6)$	107 999	33	1–19	1.7(2)	$1.74-0.0025x+(9.4\times10^{-6})x^2$			0.09(2)
$b(10)$	108 372	51	1–19	11(1)	$10.9-0.0060x$		[b]	0.05(1)
$c_4'(2)$	108 544	29	0–19	1.2(1)	P: $1.20-0.0038x+(1.2\times10^{-5})x^2$ R: $1.20+0.011x-(1.9\times10^{-5})x^2$			0.008(1)
$c_3(2)$	108 693	60	1–26	11(1)	Q: $10.6+(2.9\times10^{-3})x+(3.2\times10^{-5})x^2$ P: $10.6+0.028x-(2.5\times10^{-5})x^2$ R: $10.6-0.023x+(8.8\times10^{-5})x^2$	0.13(5)	[c]	0.09(1)
$b'(7)$	108 952	27	1–19	0.51(5)	P: $0.51-(9.5\times10^{-3})x+(5.0\times10^{-5})x^2$ R: $0.51+(6.8\times10^{-4})x-(2.3\times10^{-6})x^2+(1.1\times10^{-8})x^3$		[d]	
$b(11)$	109 120	52	1–19	4.4(4)	$4.44-(7.1\times10^{-3})x$	0.35(5)		0.33(3)
$b'(8)$	109 544	31	1–20	4.0(4)	$4.02-(4.0\times10^{-3})x$			0.025(3)
$o_3(2)$[e]	109 560	57	1–24	14(2)	$14.2+(1.01\times10^{-2})x$	0.26(5)	[f]	
$b(12)$	109 831	48	1–24	3.0(3)	$3.03-(1.6\times10^{-4})x-(1.6\times10^{-5})x^2$			0.058(5)
$b'(9)$	110 197	47	1–27	8.7(9)	$8.68+(3.4\times10^{-3})x-(4.5\times10^{-5})x^2+(5.9\times10^{-8})x^3$			<0.03
$b(13)$	110 529	47	1–22	3.1(3)	3.06	0.23(5)		
$c_4'(3)$	110 656	48	0–28	7.8(8)	P: $7.81+(6.7\times10^{-3})x$ R: $7.81+(3.0\times10^{-2})x-(6.5\times10^{-5})x^2+(4.5\times10^{-8})x^3$			0.030(6)
$c_3(3)$	110 796	37	1–20	1.0(1)	Q: $1.02+(1.7\times10^{-4})x$ P: $1.02+(9.2\times10^{-2})x-(9.4\times10^{-4})x^2+(5.0\times10^{-6})x^3-(9.7\times10^{-9})x^4$ R: $1.02-(6.9\times10^{-2})x+(1.7\times10^{-3})x^2$	0.36(5)		
$b'(10)$	110 943	26	1–21	4.2(4)	$4.18-(2.8\times10^{-2})x+(5.6\times10^{-5})x^2$			
$b(14)$	111 210	51	1–21	3.0(3)	$2.97-(6.0\times10^{-4})x$	0.21(5)	$0.21-(2.3\times10^{-4})x$	
$o_3(3)$[g]	111 448	43	1–22	8.8(9)	Q: $8.75+(1.5\times10^{-3})x$	~0.1		
$b'(11)$[h]	111 581	46	0–27	13(1)	$13.4-(4.5\times10^{-3})x-(8.7\times10^{-6})x^2$			

[a]Line intensities, which are strongly affected by two-level interference effects in the $o_3(1)$ and $b(9)$ levels, are not well represented by polynomial fits; see Ref. 51 and Sec. IV.
[b]Line broadening observed in Q and R branches for $J>14$ and $J>15$, respectively.
[c]Line broadening observed in all branches for $J>16$.
[d]Line broadening observed in the branch for $J>15$.
[e]Intensities decrease dramatically for $J>21$; linear fit is valid for $J<22$.
[f]Anomalous line width pattern for $J>12$; see Sec. IV.
[g]Anomalous P- and R-branch intensities; polynomial fit is only valid for Q branch. See Sec. IV.
[h]Anomalous P- and R-branch intensities; polynomial fit not valid for $11<J<17$. See Sec. IV.

III. ANALYSES

Absorption spectra were first converted to *measured* absorption cross sections through application of the Beer-Lambert law

$$\sigma_{exp}(\lambda)=\frac{1}{N}\ln\left[\frac{I_0(\lambda)}{I(\lambda)}\right], \quad (1)$$

where $\sigma_{exp}(\lambda)$, the experimental absorption cross section, includes the effects of the finite instrument resolution; N is the column density of N_2 molecules; $I_0(\lambda)$ is the background continuum level; and $I(\lambda)$ is the transmitted intensity. A correction for scattered light in the spectrometer, known to be less than 3% of $I_0(\lambda)$,[54] was not applied to the data. A representative experimental absorption cross section spectrum is shown in Fig. 1.

For each unblended line within a band, a least-squares fitting routine that accounts for the effects of the finite instrumental resolution was used to determine a value for the corrected integrated cross section. The background continuum level was established by sampling regions of negligible absorption between lines. Any variations in $I_0(\lambda)$ across individual lines were modeled in the fits by linear interpolation. All rotational lines were modeled with Voigt profiles. The Gaussian component is the room-temperature Doppler width of 0.24 cm^{-1} FWHM. For bands with appreciably broadened lines (Lorentzian component greater than ~0.10 cm^{-1} FWHM), the Lorentzian component of each rotational line profile was determined from the least-squares fit. For most other bands, published values from laser-based measurements[38,41,43–45,48] were used to fix the Lorentzian component in the fitting routine. Predissociation line widths in four bands, terminating on the $b'(8)$, $b'(10)$, $o_3(3)$, and $b'(11)$ levels, were too narrow to be determined by our fitting procedure and there are no available laser-based measurements; for these bands the Lorentzian component was

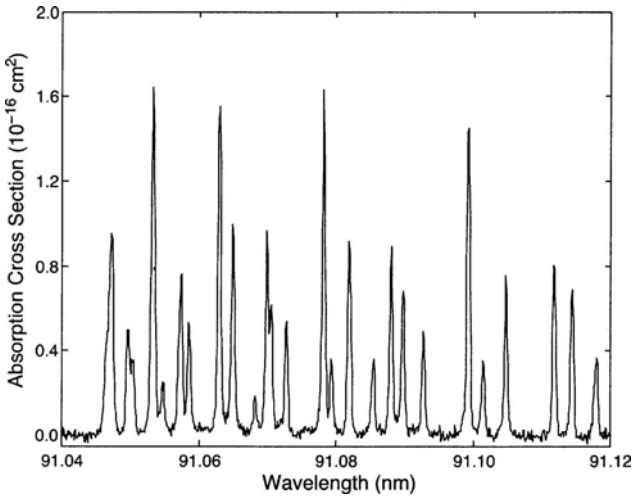

FIG. 1. Representative experimental photoabsorption cross section of the $b(12)-X(0)$ band head region at 295 K. Because of instrumental distortion of the lines, the measured peak cross sections are lower limits to the correct values.

allowed to vary in width in the range of 0.0–0.1 cm^{-1}, but the fitted values are not reported in our compilation of results.

The instrument function was also represented by a Voigt profile. Its parameters, a Gaussian width of 0.53 cm^{-1} FWHM and a Lorentzian width of 0.23 cm^{-1} FWHM, were determined by least-squares fits to the unblended lines of bands that show minimal broadening. The instrument function was adjusted locally, by marginal amounts, from fits to known narrow lines in the local spectral regions of each scan. From the distribution of fitting results, we estimate that the Gaussian and Lorentzian components of the adopted instrument Voigt profile have uncertainties of about ± 0.05 cm^{-1}.

The integrated cross sections of individual rotational lines, determined from the fitting procedure, were converted into line oscillator strengths according to[55]

$$f_{J',J''} = \left(\frac{4\varepsilon_0 m_e c^2}{e^2}\right)\frac{\int\sigma(\lambda)d\lambda}{\lambda^2\alpha_{J''}} = (1.13\times 10^3)\frac{\int\sigma(\lambda)d\lambda}{\lambda^2\alpha_{J''}}, \tag{2}$$

where $\sigma(\lambda)$ and λ are measured in units of 10^{-16} cm^2 and nm, respectively, and $\alpha_{J''}$ is the fractional population of N_2 molecules in the J'' rotational level as determined from a normalized Boltzmann factor based on N_2 ground-state term values,[56] and taking into account the 2:1 statistical weights of even- and odd-numbered levels due to nuclear spin. Uncertainties in the N_2 column densities, the adopted instrument profile of the spectrometer, and the parameters extracted from the least-squares fitting routine all contribute to the estimated uncertainties in individual line f values and widths. Column density uncertainties are estimated to range from about 5% for the highest-pressure scans to about 10% for the lowest-pressure scans. The uncertainties in the adopted instrument profile, discussed above, produce f-value uncertainties that range from 5% to 10% and produce line width uncertainties that are roughly equivalent to the instrument profile uncertainty ($\sim$0.05 cm^{-1}). For narrow features, the uncertainties in the literature values of the line widths produce very small uncertainties in our measured f values, typically less than 1%. The total uncertainties in individual line f values from all sources, including statistical uncertainties of the fitting parameters (typically $<10\%$), are estimated to range from 10% to 30% (1 standard error). For any one line in a given band, the f values derived from separate absorption scans were generally found to scatter within narrower limits. Line width uncertainties for the five bands with measurably broadened features vary quite widely, depending on the quality of the data and the relative widths of the lines.

For a small subset of the bands measured in this study, the rotational line f values follow the simple patterns associated with unperturbed transitions. In particular, for unperturbed $^1\Sigma-{}^1\Sigma$ and $^1\Pi-{}^1\Sigma$ transitions, the band oscillator strength f is related to rotational line oscillator strengths $f_{J',J''}$ by[55]

$$^1\Sigma - {}^1\Sigma\text{: } f = \frac{(2J''+1)f_{J',J''}}{S_{J',J''}}, \tag{3}$$

$$^1\Pi - {}^1\Sigma\text{: } f = \frac{2(2J''+1)f_{J',J''}}{S_{J',J''}}, \tag{4}$$

where the $S_{J',J''}$ are Hönl-London factors. For unperturbed bands, the band f values derived from the application of Eqs. (3) and (4) to measured line f values are independent of the rotational quantum number J and can be directly compared with theoretical results that neglect all rotational interactions. Most bands in this study display anomalous P-, Q-, and R-branch intensity patterns and are characterized by a marked J dependence of band f values derived from Eqs. (3) and (4). The detailed f-value patterns associated with specific bands are presented in Sec. IV. For transitions from the ground state of N_2, it is the upper-state wave function that is responsible for all departures from the standard line strength formulas. Accordingly, the band f values derived from Eqs. (3) and (4) are considered as functions of J'. To facilitate comparisons with calculated band strengths, we represent the derived band $f(J')$ values as simple polynomials in $J'(J'+1)$ that are to be used for extrapolation to $J'=0$. We refer to the band f values extrapolated to $J'=0$ as "rotationless" band f values. The J dependences of measured line widths are treated in the same manner.

When particularly relevant to the analysis of a band, the f values and/or predissociation line widths of blended pairs or groups of lines were determined by the least-squares fitting procedure. In these cases, the ratios of line f values of the blended features were fixed using either Hönl-London factors and Boltzmann factors or by interpolation of f values within a branch, and line widths of the blended features were tied to a common value. For some blended and/or weak features it was not possible to determine simultaneously the f value and the line width. In these cases, the line f value was fixed by measured f values in other branches at the same J value or by an interpolation of f values within a branch, and the line width was determined by the fitting procedure, or, alternatively, the line width was fixed and the line f value allowed to vary in the fitting procedure.

TABLE II. Comparison of band oscillator strengths ($\times 10^3$) for EUV transitions of $^{14}N_2$. Uncertainties (1 standard error; in parentheses) are in units of the last-quoted decimal place. The band f values of column 2 are "rotationless." f values in columns 3–5 are strictly appropriate for room temperature only.

Band	This work	Ref. 20[a]	Ref. 32[b]	Refs. 33 and 34[a]	Ref. 16[a]	Ref. 21
$b'(5)-X(0)$	1.1(1)	0.92		0.18	0.94	1.2
$o_3(1)$	3.0(3)				26	7.3
$b(9)$	14(2)	21[c]	26[c]	3.9	5.6	16
$b'(6)$	1.7(2)	1.9	2.2	3.3	1.4	1.9
$b(10)$	11(1)	11	14.7	12	9.2	15
$c_4'(2)$	1.2(1)			3.4	1.2	1.4
$c_3(2)$	11(1)	13	15.5		8.2	14
$b'(7)$	0.51(5)			4.3	0.19	0.45
$b(11)$	4.4(4)	3.7	4.8	4.0	5.1	6.8
$b'(8)$	4.0(4)			28	2.7	4.4
$o_3(2)$	14(2)	21	28		24	19
$b(12)$	3.0(3)	0.72	1.8	0.9	1.7	4.3
$b'(9)$	8.7(9)	5.9	12.8	12	6.5	10.4
$b(13)$	3.1(3)				2.5	4.5
$c_4'(3)$	7.8(8)	1.2	19	18	6.5	9.6
$c_3(3)$	1.0(1)				0.97	1.7
$b'(10)$	4.2(4)	1.0		2.0	3.4	5.2
$b(14)$	3.0(3)	0.73	5.1[d]	1.0	4.6	4.6
$o_3(3)$	8.8(9)	19	24		12	10.2
$b'(11)$	13(1)	2.1?	6.5	4.4	11	16

[a] f values normalized to $f=0.043$ for $b(3)-X(0)$ (Ref. 12).
[b] Uncertainties of 10%–20%.
[c] Sum of $o_3(1)-X(0)$ and $b(9)-X(0)$ f values.
[d] Sum of $b'(10)-X(0)$ and $b(14)-X(0)$ f values.

IV. RESULTS AND DISCUSSION

A summary of our measurements and analyses is presented in Table I; all electric-dipole-allowed N_2 transitions between 89.7 and 93.5 nm are included. For completeness, the table includes the corresponding data for the $b(9)-X(0)$ and $o_3(1)-X(0)$ bands, for which a detailed analysis is presented in Vieitez *et al.*[51] A detailed listing of measured f values and widths for individual rotational lines can be accessed through Ref. 57. Table II compares the rotationless band f values of the second column with band f values derived from electron energy-loss measurements,[20,32] electron-impact studies of emission-excitation cross sections,[33,34] and calculations based on sets of electronically coupled diabatic potential curves.[16,21] Except for the present work and the calculated f values in the last two columns, all other data in the table are strictly valid only for a room-temperature distribution of rotational populations.

There is reasonable agreement between our rotationless band f values and the normalized f values of Geiger and Schröder[20] for bands above ~91.2 nm, but far less agreement at shorter wavelengths. For a number of bands, the f values of Geiger and Schröder[20] are a factor of 4 or more smaller than our rotationless band f values, a trend that is not explained by the J dependence of the line strengths (see Table I). The difficulties of extracting the strengths of closely spaced bands in the relatively low-resolution (~80 cm^{-1} FWHM) electron energy-loss spectrum are apparent in the $o_3(3)-X(0)$ and $b'(11)-X(0)$ bands, for which Geiger and Schröder[20] report f values of 19×10^{-3} and 2×10^{-3}, respectively, the latter albeit uncertain, and we report rotationless f values of 9×10^{-3} and 13×10^{-3}; while the individual band f values are significantly discrepant, the sums of the f values are in good agreement.

The f values reported by Chan *et al.*[32] from electron-energy-loss spectra are, with one or two exceptions, consistently higher than our results. The sum of their reported band f values throughout the 89.7–93.5 nm region is 35% higher than the corresponding sum of rotationless band f values reported in this paper. The low resolution of the electron scattering spectra (~400 cm^{-1} FWHM) may explain some of the individual discrepancies; extraction of f values requires the deconvolution of highly blended features in the energy-loss spectrum (see Fig. 5 of Ref. 32). However, the systematic discrepancy between the two sets of results cannot be explained by the low resolution of the electron-energy-loss spectra. Chan *et al.*[32] note correctly that their f values for resolved features are insensitive to the instrumental resolution, as opposed to the case for photoabsorption measurements. Nevertheless, the present results have been corrected for instrumental effects and are inherently *absolute*. The results of Chan *et al.*,[32] in contrast to the other experimental results used for comparison here,[20,33,34] do not rely on a calibration against an optical oscillator strength, but are subject to an energy-dependent Bethe-Born apparatus calibration factor and overall Thomas-Reiche-Kuhn sum-rule normalization.[32] At present, the reason for the 35% discrepancy, which lies somewhat outside the combined uncertainties, is unclear.

There is very poor agreement between the present f values and the rescaled f values of Ajello *et al.*[33] and James

et al.,[34] which were obtained from electron-impact-induced emission spectra. These latter results, are, on average, a factor of ~2 larger than the present values, with differences of around an order of magnitude in either direction for particular bands.

The calculations of Stahel *et al.*[16] and of Spelsberg and Meyer,[21] neither of which accounts for rotational interactions, can be directly compared with our rotationless band f values. The f values derived from the *ab initio* calculations of Spelsberg and Meyer,[21] shown in the last column of Table II, are, on average, ~20% higher than the present measurements in the case of the $^1\Sigma_u^+ - X(0)$ transitions and ~40% higher in the case of the $^1\Pi_u - X(0)$ transitions. However, there is excellent agreement between the two data sets for the *relative* vibrational dependences of the f values. Since we have renormalized the results of Stahel *et al.*[16] using a more recent and accurate optical oscillator strength[12](see Table II), their f values are in better *systematic* agreement with the present measurements than are those of Spelsberg and Meyer,[21] but there are significantly more individual inconsistencies. Furthermore, since the model of Stahel *et al.*[16] was optimized by fitting their calculated coupled-channel intensities to the relative electron-energy-loss spectra of Geiger and Schröder,[20] whose intensities represent measurements over *room-temperature* rotational populations and show some strong deviations from our results, departures of the results of Stahel *et al.*[16] from our measured rotationless f values can be expected.

Overall, the excellent agreement between the apparently chaotic vibrational dependences of the present f values and those implied by the *ab initio* calculations of Spelsberg and Meyer[21] is very encouraging, both with respect to the reliability of the present results and correctness of the coupled-state interference effects in the calculations of Spelsberg and Meyer.[21] It is to be hoped that the present results, especially the detailed rotational dependences, will aid in the further development of the semiempirical CSE models for N_2.[22,23]

The following paragraphs provide a band-by-band summary and a discussion of our observations in the 89.7–93.5 nm region.

$b'(5) - X(0)$. Band f values derived from the two branches of this sharp band converge to a common rotationless f value and were fit separately to linear functions of $J'(J'+1)$. The P/R ratios of the line f values deviate somewhat from predictions based on Hönl-London factors, though not dramatically. The sum of line f values for P and R transitions from a common J'' level is J'' independent.

$o_3(1) - X(0)$, $b(9) - X(0)$. Absorption spectra of the $o_3\,^1\Pi_u(1) \sim b\,^1\Pi_u(9)$ Rydberg-valence complex are characterized by perturbed rotational structures and significant quantum-interference effects in oscillator-strength patterns and predissociation line widths. A detailed analysis of the $o_3(1) - X(0)$ and $b(9) - X(0)$ bands, based on a two-level perturbation model, is presented by Vieitez *et al.*[51] That analysis was derived from a combination of laser-based ionization spectroscopy of $^{14}N_2$ and $^{14}N^{15}N$ and the synchrotron-based $^{14}N_2$ photoabsorption spectra reported here. Line f values and line widths for 43 features in the $b(9) - X(0)$ band and 58 features in the $o_3(1) - X(0)$ band are catalogued in Ref. 57 as a complement to the data presented by Vieitez *et al.*[51] Band f values derived from line f values are branch independent in both bands. A strong two-level quantum-interference effect is observed in the f-value patterns. Transition strengths to the higher-energy levels peak near $J'=6$ and transition strengths to the lower-energy levels follow a complementary pattern, with transitions to $J'=6$ being too weak to be observed. Measured predissociation line widths in the absorption spectra range from 0.1 to 0.4 cm^{-1} FWHM. Line width patterns, as revealed by the combination of laser-based and synchrotron data, exhibit a somewhat weaker interference pattern than seen in the f-value data, suggesting an additional interaction with a third, repulsive state.[51]

$b'(6) - X(0)$. With the exception of the $R(3)$ line, the P- and R-branch lines in this band are blended until $P(10)$ and $R(13)$. f values for the blended features were determined by fixing the ratio of line f values using Hönl-London factors and Boltzmann factors. There is a weak J dependence in the derived band f values. Fitted predissociation line widths vary from 0.05 to 0.20 cm^{-1} FWHM, roughly consistent with the low-J line width of 0.09 cm^{-1} FWHM reported by Sprengers and Ubachs[48] from laser-based measurements. Because of the large uncertainties in our fitted line widths, we do not include these values in our band compilation. The interaction of the $b'(6)$ rotational levels with those of the $o_3(1)$ and $b(9)$ states (Vieitez *et al.*[51]), which should lead to conspicuous line strength anomalies near the $b'(6) - o_3(1)$ crossing between $J=24$ and $J=25$, is not evident in our lower-J spectra.

$b(10) - X(0)$. The rotational structure of this band allows for a fairly complete set of line f-value measurements in all three branches; a total of 51 line f values were determined. All band f values determined from line f values follow the same linearly decreasing function of $J'(J'+1)$. This simple, branch-independent intensity pattern allowed for the inclusion of blended lines in the line f-value compilation; the ratio of f values of blended lines was fixed in the fitting procedure by Hönl-London factors and Boltzmann factors. Predissociation line widths were fixed at 0.05 cm^{-1} FWHM (Ref. 48) until the onset of observable broadening in the highest-J lines. Measured line widths for the $Q(15)$ through $Q(18)$ and $R(16)$ through $R(18)$ lines increased from 0.1 to 0.5 cm^{-1} FWHM. There is some evidence for more significant broadening, up to ~1.0 cm^{-1} FWHM, in the $R(19)$, $R(20)$, and $Q(19)$ lines, but the weakness of the features precludes definitive width measurements. A photographic plate of room-temperature absorption through a high column density of N_2, recorded on the 6.65 m vacuum spectrometer at the Harvard-Smithsonian Center for Astrophysics with a helium continuum light source,[58] qualitatively confirms the broadening pattern seen in our spectra and indicates that the broadening diminishes by $Q(21)$. Carroll and Collins[15] report an anomalous increase in the intensity of lines with $J \approx 18$; this may be a reflection of the line broadening observed in our spectra.

$c_4'(2) - X(0)$. The rotationless band f value was determined from a quadratic fit of measured low-J P-branch f values to $J'(J'+1)$. f values derived from the R branch, for which only higher-J lines were measured, were fit separately to a quadratic function of $J'(J'+1)$ with the rotationless f value held fixed. While quadratic fits to $J'(J'+1)$ are re-

quired to describe the f values in both branches, no extreme departures from standard line strength patterns are observed over the range of J values measured. Yoshino *et al.*[59] and Ubachs *et al.*[41] discuss the spectroscopy of $c_4'(2)$ and identify strong homogeneous interactions with nearby vibrational levels of the b' state, predominantly $b'(7)$ and $b'(6)$, as well as mixing with the $c_3(2)$ level. Ubachs *et al.*[41] account for radiative lifetime variations in the band via Rydberg-valence mixing in the $^1\Sigma_u^+$ manifold.

$c_3(2)-X(0)$. f values for 60 lines in this band were determined over a range of J' values from 1 to 26. The band f values derived from the Q-branch lines, which show a mild J' dependence, were first fit to a quadratic function of $J'(J'+1)$ to yield the rotationless band f value. The corresponding R-branch and P-branch data were then fit to polynomial functions of $J'(J'+1)$ with the $J'=0$ intercept held fixed at the rotationless band f value. The P/R ratios of the line f values deviate somewhat from predictions based on Hönl-London factors, with P-branch lines being about 20% to 30% stronger than the corresponding R-branch lines. The line f values for P and R transitions from a common J'' level sum to the f value for the corresponding Q line. Sprengers and Ubachs[48] report lifetime measurements of the $c_3(2)$ level that correspond to predissociation line widths of ~ 0.1 cm^{-1} FWHM. Our fitted predissociation line widths are consistent with this value for all lines with $J'<17$. Line broadening is seen in all three branches for $J'>16$, with maximum values of about 1.0 cm^{-1} FWHM near $J'=21$.

$b'(7)-X(0)$. This weak band is overlapped by the stronger $b(11)-X(0)$ band, but a number of lines in each branch could be measured. A striking feature of the band is the rapidly decreasing strength of the P-branch lines with increasing rotational quantum number; the highest-J line observed was $P(11)$. Conversely, the R-branch lines begin to increase in strength when $J'>12$. At low J values, the band f values derived from lines within the P and R branches converge to a common rotationless value of 0.000 51(5). Predissociation line widths for all but the highest-J lines were too narrow to be extracted from the data; no previous line width or lifetime measurements are available. Line broadening was observed in the highest-J lines of the R branch, growing to ~ 0.5 cm^{-1} FWHM for the $R(18)$ line. The large difference between the R- and P-branch band f values observed for the $b'(7)-X(0)$ transition is a classical example of the interference-induced R/P intensity anomalies that may occur in transitions to mixed $\Sigma\sim\Pi$ levels.[60] In the present case, the nominal $b'^1\Sigma_u^+(v=7)$ level gains significant $^1\Pi_u$ character from a heterogeneous perturbation by the $c_3(2)$ level, leading to a strong R/P intensity anomaly,[61] due to interference between the corresponding parallel ($\mu^{\parallel}$) and perpendicular ($\mu^{\perp}$) vibronic transition moments.

$b(11)-X(0)$. Line strengths and widths of 52 lines of this band were measured. As in the $b(10)-X(0)$ band, band f values derived from line f values in the three branches follow a common, linearly decreasing function of $J'(J'+1)$. The branch-independent intensity pattern simplifies the analysis of blended lines, which are included in our line f-value compilation. All lines are noticeably broadened; a J-independent and branch-independent predissociation line width of ~ 0.35 cm^{-1} FWHM is found, in excellent agreement with the laser-based measurements of Ubachs *et al.*[38] There is significant spectral overlap between rotational features in the $b(11)-X(0)$ band and the bright N II feature at 91.6 nm ($2p^{33}p^0\rightarrow 2p^{23}P$ sextuplet) observed in the Earth's airglow;[62,63] the line strengths and profiles in $b(11)-X(0)$ will influence the loss of airglow photons through reabsorption by N_2.

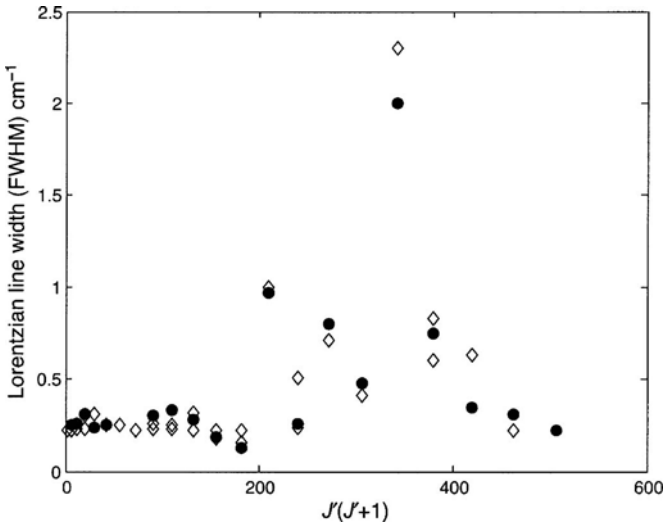

FIG. 2. Experimentally determined Lorentzian component of line widths (FWHM) in the $o_3(2)-X(0)$ band [P and R branches (open diamonds) and Q branch (solid circles)]. The anomalous line-width patterns exhibit sharply peaked values at $J'=18$ after two lesser peaks at $J'=14$ and $J'=16$ (see text).

$b'(8)-X(0)$. This band is overlapped with the stronger $o_3(2)-X(0)$ band; 31 rotational lines, including a number of blended features, were analyzed. Band f values derived from P- and R-branch line f values follow a common, linearly decreasing function of $J'(J'+1)$. There is no noticeable broadening in photographic plates of the band, and our fitted predissociation line widths, while too narrow to be determined definitively, are consistently <0.1 cm^{-1} FWHM.

$o_3(2)-X(0)$. 57 lines in this strong band, including a substantial number of blended features, were analyzed for strengths and widths. Band f values derived from line f values in the three branches follow a common, linearly increasing function of $J'(J'+1)$ up to $J'\approx 21$. The Q branch could be followed up to $J=24$. Line strengths in the three highest-J lines depart significantly from the simple pattern; they are approximately 50% lower than predicted by the linear function of $J'(J'+1)$. Predissociation line widths associated with e-parity and f-parity levels[60] remain constant, at ~ 0.25 cm^{-1} FWHM, up to $J'=12$. Beyond this point the line-width pattern is strikingly anomalous, reaching a peak value of ~ 2 cm^{-1} FWHM at $J'=18$ after two lesser peaks at $J'=14$ and $J'=16$, as seen in Fig. 2. These line-width perturbations, which occur in both the e- and f-parity levels, suggest that $o_3(2)$ is crossed by a predissociative triplet level having $\Lambda\geqslant 1$. An extrapolation of recent results at lower transition energies[26,64] suggests that the perturber is the $v=18$ level of the $C^3\Pi_u$ state, which is itself predissociated by the $C'^3\Pi_u$ valence continuum.

$b(12)-X(0)$. Band f values derived from line f values in the three branches follow a common, quadratically decreasing function of $J'(J'+1)$ up to $J' \approx 19$. Only one line with $J' > 19$ was observed and measured, the $Q(24)$ line, which is found within the band structure of $o_3(2)-X(0)$ and has a much larger f value than predicted by the pattern at lower values of J. This deviation likely reflects the avoided crossing between the $b(12)$ and $o_3(2)$ levels described by Yoshino *et al.*[19] and complements the loss in intensity seen in the high-J lines of the $o_3(2)$ Q branch. Predissociation line widths, which were reported to be 0.05 cm^{-1} FWHM by Hanneman *et al.*,[45] were too narrow to be analyzed in our data.

$b'(9)-X(0)$. All lines in the P and R branches of this sharp band up to $J' \sim 23$ were measured and analyzed. Ratios of band f values derived from the two branches are consistent with Hönl-London factors, and the derived band f value displays a weak dependence on rotational quantum number. Predissociation line widths, which were reported to be <0.03 cm^{-1} FWHM by Ubachs *et al.*,[38] were too narrow to be analyzed in our data.

$b(13)-X(0)$. 47 lines were measured in the three branches with J' values up to 21. Band f values derived from line f values are branch independent and J independent. All lines show evidence of broadening. Predissociation line widths are branch and J independent, with an average value of 0.23 cm^{-1} FWHM.

$c_4'(3)-X(0)$. A total of 48 lines in the P and R branches of this band were analyzed for f values. The $c_4'(3)$ level is known to be strongly mixed with the $c_3(3)$ and $b'(10)$ levels.[33,49,52,59] Our derived band f values from each branch trend gradually upwards from a common rotationless value; with the P-branch values slightly higher than the R-branch values at intermediate J. The branch-averaged pattern is consistent with the calculated photoexcitation line strengths for the $c_4'(3)-a''^1\Sigma_g^+(0)$ band of Walter *et al.*[49] (see Fig. 6a of Ref. 49), who attribute the J-dependent increase in line strength to a gradual increase in the fractional b' character of the $c_4'(3)$ rotational levels with increasing J. Predissociation line widths, which were reported to range from 0.020 to 0.036 cm^{-1} FWHM for $0 \leqslant J' \leqslant 15$ by Kam *et al.*,[65] were too narrow to be measured with our apparatus.

$c_3(3)-X(0)$. Band f values derived from 18 lines in the Q branch of this weak band are independent of J, and were used to establish the rotationless band f value of 1.0×10^{-3}. Line strengths in the P and R branches display extreme departures from nominal $\Pi-\Sigma$ patterns, as demonstrated in Fig. 3. Band f values derived from P-branch line strengths increase dramatically with J', from a minimum value of 1×10^{-3} for low-J lines to a maximum of 6×10^{-3} near $J' = 14$. A steep decrease in band f values is observed in the highest-J measured P-branch lines. R-branch band f values decrease abruptly from the common rotationless value and the branch cannot be followed in our spectra beyond $J' = 4$. Line widths in all three branches are consistently broadened, with an average, J-independent value of ~ 0.35 cm^{-1} FWHM. The calculated $c_3(3)-a''(0)$ line strengths of Walter *et al.*[49] show a similar overall pattern to our $c_3(3)-X(0)$ observations, with the branch-averaged line strength peaking near $J' = 14$: the pattern is attributed to J-dependent intensity borrowing from the $b'(10)-X(0)$ transition. Walter *et al.*[49] also note a significant difference in P- and R-branch photofragment intensities, but they describe the R-branch transitions as being considerably stronger than the P-branch transitions.

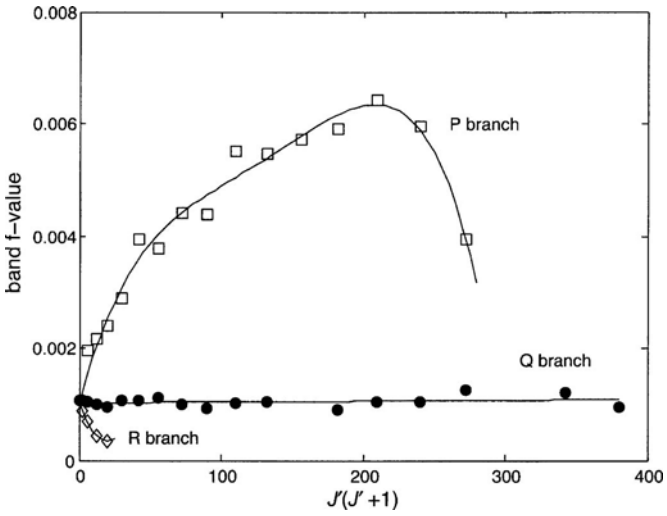

FIG. 3. $c_3(3)-X(0)$ band f values determined from rotational line f values and Hönl-London factors [P branch (open squares), Q branch (solid circles), and R branch (open diamonds)]. The J dependence of the Q-branch f values is adequately represented by a linear fit to $J'(J'+1)$; P-branch and R-branch f values, which display significant P/R intensity anomalies (see text), are fit to higher order polynomials with a common rotationless intercept fixed by the Q-branch intercept.

The large difference between the P- and R-branch f values observed for the $c_3(3)-X(0)$ transition in Fig. 3 indicates another extreme case of an R/P intensity anomaly in transitions to mixed $\Sigma \sim \Pi$ levels. In this case, the nominal $c_3\,^1\Pi_u(v=3)$ level borrows significant $^1\Sigma_u^+$ character from the $b'(10)$ level and the corresponding $\mu^\perp \sim \mu^\parallel$ interference effect is of the opposite sense to that described above for the $b'(7)-X(0)$ transition. To explain the remarkable change in sense of the R/P intensity anomaly for the transition to the *same mixed upper level*, achieved simply by changing the initial level from the present $X(0)$ to the $a''(0)$ of Walter *et al.*,[49] it is necessary to note that the relevant interference term is proportional to $\mu^\parallel\mu^\perp$.[60] Evidently, the vibronic product $\mu^\parallel\mu^\perp$ has different signs for the $c_3(3)-X(0)$ and $c_3(3)-a''(0)$ transitions.

$b'(10)-X(0)$. 27 lines were analyzed in this band. Line strengths in the P and R branches decrease approximately linearly with $J'(J'+1)$ until becoming almost indiscernible near $J' \approx 16$. This pattern is consistent with the photofragment intensity pattern described by Walter *et al.*[49] for $0 \leqslant J' \leqslant 17$. We observe higher-$J'$ lines in the P branch within the structure of the nearby $c_3(3)-X(0)$ band. Despite the relatively large uncertainties in the f values of these lines, it is clear that they are gaining significant strength with increasing J'. This may be attributable to the rapidly increasing fractional b-state character in the $b'(10)$ rotational levels, with an onset at $J \approx 20$, described by Walter *et al.*[49] Predissociation line widths throughout the band appear to be in the range of 0.05 to 0.15 cm^{-1} FWHM, generally too small to be definitively measured with our apparatus.

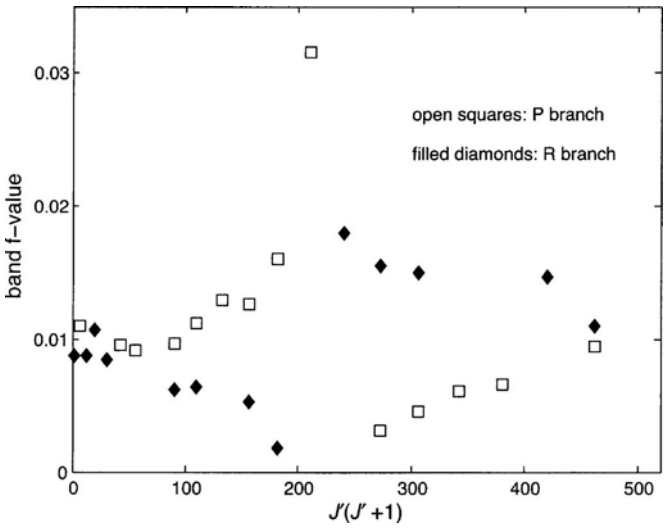

FIG. 4. $o_3(3)-X(0)$ band f values determined from rotational line f values and Hönl-London factors for the P (open squares) and R (solid diamonds) branches. A crossing with $b'(11)$ at $J\sim 14.5$ results in strongly anomalous line strength patterns in the P and R branches. Strengths in both branches display characteristic interference patterns associated with the crossing, with the sign of the interference reversed in the two branches. Q branch f values, not shown for clarity, are ~0.010 and are approximately independent of J'.

$b(14)-X(0)$. Band f values derived from 51 measured line f values are branch independent and display a slight linear dependence on $J'(J'+1)$. All lines show evidence of broadening. The branch-independent predissociation line widths have a rotationless value of 0.21 cm^{-1} FWHM and decrease linearly with $J'(J'+1)$ to 0.12 cm^{-1} FWHM at $J'=16$.

$o_3(3)-X(0)$. Despite numerous blends with $b'(11)-X(0)$ features, 47 lines were analyzed for strengths and widths. Band f values derived from Q-branch line strengths are almost independent of $J'(J'+1)$. P-branch and R-branch line strengths are consistent with Q-branch line strengths for the lowest and highest J values measured. A crossing with $b'(11)$ at $J\approx 14.5$, first analyzed by Yoshino *et al.*,[19] results in a strongly anomalous line strength pattern in the P and R branches in this region. Strengths in both branches display characteristic interference patterns, with the sign of the interference reversed in the two branches, as demonstrated in Fig. 4. Predissociation line widths in all three branches appear to be in the range of 0.05 to 0.15 cm^{-1} FWHM, which is at the lower limit of our analysis capabilities.

$b'(11)-X(0)$. Except in the region of the crossing with $o_3(3)$, band f values in both branches decrease with increasing J'; a quadratic fit to $J'(J'+1)$ is needed to describe the f-value pattern. P- and R-branch f values display interference patterns at the crossing ($J'\approx 14.5$), with each branch f-value pattern complementing the corresponding branch pattern in the $o_3(3)-X(0)$ band. Predissociation line widths are too narrow to be determined with our apparatus.

ACKNOWLEDGMENTS

This work was supported in part by NASA Grant No. NNG05GA03G to Wellesley College and Australian Research Council Discovery Program Grant No. DP0558962. The measurements were carried out under the approval of the Photon Factory Advisory Committee (Proposal No. 1998G245). We thank the staff of the Photon Factory for their hospitality and assistance.

[1] R. R. Meier, Space Sci. Rev. **58**, 1 (1991).
[2] P. D. Feldman, D. J. Sahnow, J. W. Kruk, E. M. Murphy, and H. W. Moos, J. Geophys. Res. **106**, 8119 (2001).
[3] J. Bishop and P. D. Feldman, J. Geophys. Res. **108**, 1243 (2003).
[4] D. F. Strobel and D. E. Shemansky, J. Geophys. Res. **87**, 1361 (1982).
[5] M. H. Stevens, R. R. Meier, R. R. Conway, and D. F. Strobel, J. Geophys. Res. **99**, 417 (1994).
[6] M. H. Stevens, J. Geophys. Res. **106**, 3685 (2001).
[7] A. L. Broadfoot, S. K. Atreya, J. L. Bertaux, J. E. Blamont, A. J. Dessler, T. M. Donahue, W. T. Forrester, D. T. Hall, F. Herbert, J. B. Holberg, D. M. Hunten, V. A. Krasnopolsky, S. Linick, J. I. Lunine, J. C. McConnell, H. W. Moos, B. R. Sandel, N. M. Schneider, D. E. Shemasnsky, G. R. Smith, D. F. Strobel, and R. V. Yelle, Science **246**, 1459 (1989).
[8] D. C. Knauth, B.-G. Andersson, S. R. McCandliss, and H. W. Moos, Nature (London) **429**, 636 (2004).
[9] V. Vuitton, R. V. Yelle, and V. G. Anicich, Astrophys. J. Lett. **647**, L175 (2006).
[10] M.-C. Liang, A. N. Heays, B. R. Lewis, S. T. Gibson, and Y. L. Yung, Astrophys. J. Lett. **664**, L115 (2007).
[11] R. J. Vervack, B. R. Sandel, and D. F. Strobel, Icarus **170**, 91 (2004).
[12] G. Stark, K. P. Huber, K. Yoshino, P. L. Smith, and K. Ito, J. Chem. Phys. **123**, 214303 (2005).
[13] H. Lefebvre-Brion, Can. J. Phys. **47**, 541 (1969).
[14] K. Dressler, Can. J. Phys. **47**, 547 (1969).
[15] P. K. Carroll and C. P. Collins, Can. J. Phys. **47**, 563 (1969).
[16] D. Stahel, M. Leoni, and K. Dressler, J. Chem. Phys. **79**, 2541 (1983).
[17] P. K. Carroll, C. P. Collins, and K. Yoshino, J. Phys. B **3**, L127 (1970).
[18] P. K. Carroll and K. Yoshino, J. Phys. B **5**, 1614 (1972).
[19] K. Yoshino, Y. Tanaka, P. K. Carroll, and P. Mitchell, J. Mol. Spectrosc. **54**, 87 (1975).
[20] J. Geiger and B. Schröder, J. Chem. Phys. **50**, 7 (1969).
[21] D. Spelsberg and W. Meyer, J. Chem. Phys. **115**, 6438 (2001).
[22] B. R. Lewis, S. T. Gibson, W. Zhang, H. Lefebvre-Brion, and J.-M. Robbe, J. Chem. Phys. **122**, 144302 (2005).
[23] V. E. Haverd, B. R. Lewis, S. T. Gibson, and G. Stark, J. Chem. Phys. **123**, 214304 (2005).
[24] J. P. Sprengers, E. Reinhold, W. Ubachs, K. G. H. Baldwin, and B. R. Lewis, J. Chem. Phys. **123**, 144315 (2005).
[25] T. Hashimoto and H. Kanamori, J. Mol. Spectrosc. **235**, 104 (2006).
[26] B. R. Lewis, K. G. H. Baldwin, J. P. Sprengers, W. Ubachs, G. Stark, and K. Yoshino (unpublished).
[27] B. R. Lewis, personal communication (1 September 2007).
[28] X. Liu, D. E. Shemansky, C. P. Malone, P. V. Johnson, J. M. Ajello, I. Kanik, A. N. Heays, B. R. Lewis, S. T. Gibson, and G. Stark, J. Geophys. Res. (in press).
[29] V. L. Carter, J. Chem. Phys. **56**, 4195 (1972).
[30] P. Gürtler, V. Saile, and E. E. Koch, Chem. Phys. Lett. **48**, 245 (1977).
[31] G. M. Lawrence, D. L. Mickey, and K. Dressler, J. Chem. Phys. **48**, 1989 (1968).
[32] W. F. Chan, G. Cooper, R. N. S. Sodhi, and C. E. Brion, Chem. Phys. **170**, 81 (1993).
[33] J. M. Ajello, G. K. James, B. O. Franklin, and D. E. Shemansky, Phys. Rev. A **40**, 3524 (1989).
[34] G. K. James, J. M. Ajello, B. Franklin, and D. E. Shemansky, J. Phys. B **23**, 2055 (1990).
[35] M. Leoni and K. Dressler, Z. Angew. Math. Phys. **22**, 794 (1971).
[36] H. Oertel, M. Kratzat, J. Imschweiler, and T. Noll, Chem. Phys. Lett. **82**, 552 (1981).
[37] W. Ubachs, L. Tashiro, and R. N. Zare, Chem. Phys. **130**, 1 (1989).
[38] W. Ubachs, K. S. F. Eikema, and W. Hogervorst, Appl. Phys. B: Photophys. Laser Chem. **57**, 411 (1993).
[39] W. Ubachs, Chem. Phys. Lett. **268**, 201 (1997).
[40] W. Ubachs, I. Velchev, and A. de Lange, J. Chem. Phys. **112**, 5711 (2000).
[41] W. Ubachs, R. Lang, I. Velchev, W.-Ü. L. Tchang-Brillet, A. Johansson, Z. X. Li, V. Lokhnygin, and C.-G. Wahlström, Chem. Phys. **270**, 215 (2001).
[42] J. P. Sprengers, W. Ubachs, A. Johansson, A. L'Huillier, C.-G. Wahl-

ström, R. Lang, B. R. Lewis, and S. T. Gibson, J. Chem. Phys. **120**, 8973 (2004).
[43] J. P. Sprengers, A. Johansson, A. L'Huillier, C.-G. Wahlström, B. R. Lewis, and W. Ubachs, Chem. Phys. Lett. **389**, 348 (2004).
[44] J. Philip, J. P. Sprengers, P. Cacciani, C. A. de Lange, and W. Ubachs, Appl. Phys. B: Lasers Opt. **78**, 737 (2004).
[45] S. Hannemann, U. Hollenstein, E.-J. van Duijn, and W. Ubachs, Opt. Lett. **30**, 1494 (2005).
[46] J. P. Sprengers, W. Ubachs, and K. G. H. Baldwin, J. Chem. Phys. **122**, 144301 (2005).
[47] B. R. Lewis, S. T. Gibson, J. P. Sprengers, W. Ubachs, A. Johansson, and C.-G. Wahlström, J. Chem. Phys. **123**, 236101 (2005).
[48] J. P. Sprengers and W. Ubachs, J. Mol. Spectrosc. **235**, 176 (2006).
[49] C. W. Walter, P. C. Cosby, and H. Helm, J. Chem. Phys. **112**, 4621 (2000).
[50] J. M. Ajello, G. K. James, and M. Ciocca, J. Phys. B **31**, 2437 (1998).
[51] M. O. Vieitez, T. I. Ivanov, J. P. Sprengers, C. A. de Lange, W. Ubachs, B. R. Lewis, and G. Stark, Mol. Phys. **105**, 1543 (2007).
[52] S. A. Edwards, W.-Ü. L. Tchang-Brillet, J.-Y. Roncin, F. Launay, and F. Rostas, Planet. Space Sci. **43**, 67 (1995).
[53] K. Ito, T. Namioka, Y. Morioka, T. Sasaki, H. Noda, K. Goto, T. Katayama, and M. Koike, Appl. Opt. **25**, 837 (1986).
[54] K. Ito, K. Maeda, Y. Morioka, and T. Namioka, Appl. Opt. **28**, 1813 (1989).
[55] D. C. Morton and L. Noreau, Astrophys. J., Suppl. Ser. **95**, 301 (1994).
[56] S. A. Edwards, J.-Y. Roncin, F. Launay, and F. Rostas, J. Mol. Spectrosc. **162**, 257 (1993).
[57] See EPAPS Document No. E-JCPSA6-128-012806. This data archive consists of tabulations of experimentally determined line *f*-values and line widths in 20 $^{14}N_2$ bands between 89.7 and 93.5 nm. This document can be reached through a direct link in the online article's HTML reference section or via the EPAPS homepage (http://www.aip.org/pubservs/epaps.html).
[58] K. Yoshino (unpublished).
[59] K. Yoshino, D. E. Freeman, and Y. Tanaka, J. Mol. Spectrosc. **76**, 153 (1979).
[60] H. Lefebvre-Brion and R. W. Field, *The Spectra and Dynamics of Diatomic Molecules* (Elsevier, Amsterdam, 2004), pp. 144–145 and 386–403.
[61] M. O. Vieitez, T. I. Ivanov, C. A. de Lange, W. Ubachs, A. N. Heays, B. R. Lewis, and G. Stark, "Interactions of the $3p\pi_u c\ ^1\Pi_u(v=2)$ Rydberg-complex member in isotopic N_2", J. Chem. Phys. (in press).
[62] P. D. Feldman, D. J. Sahnow, J. W. Kruk, E. M. Murphy, and H. W. Moos, J. Geophys. Res. **106**, 8119 (2001).
[63] R. R. Meier, J. A. R. Samson, Y. Chung, E.-M. Lee, and Z.-X. He, Planet. Space Sci. **39**, 1197 (1991).
[64] B. R. Lewis, A. N. Heays, S. T. Gibson, H. Lefebvre-Brion, and R. Lefebvre (unpublished).
[65] A. W. Kam, J. R. Lawall, M. D. Lindsay, F. M. Pipkin, R. C. Short, and P. Zhao, Phys. Rev. A **40**, 1279 (1989).